THE ASTROPHYSICAL JOURNAL, 552:168–174, 2001 May 1

MOLECULAR CARBON CHAINS AND RINGS IN TMC-1

DAVID FOSSÉ,[1,2] JOSÉ CERNICHARO,[1] MARYVONNE GERIN,[2] AND PIERRE COX[3]

Received 2000 April 18; accepted 2001 January 3

ABSTRACT

We present mapping results in several rotational transitions of HC_3N, C_6H, both cyclic and linear C_3H_2 and C_3H, toward the cyanopolyyne peak of the filamentary dense cloud TMC-1 using the IRAM 30 m and MPIfR 100 m telescopes. The spatial distribution of the cumulene carbon chain propadienylidene H_2CCC (hereafter l-C_3H_2) is found to deviate significantly from the distributions of the cyclic isomer c-C_3H_2, HC_3N, and C_6H, which, in turn, look very similar. The cyclic over linear abundance ratio of C_3H_2 increases by a factor of 3 across the filament, with a value of 28 at the cyanopolyyne peak. This abundance ratio is an order of magnitude larger than the range (3–5) we observed in the diffuse interstellar medium. The cyclic over linear abundance ratio of C_3H also varies by $\sim$2.5 in TMC-1, reaching a maximum value (13) close to the cyanopolyyne peak. These behaviors might be related to competitive processes between ion-neutral and neutral-neutral reactions for cyclic and linear species.

Subject headings: ISM: abundances — ISM: individual (TMC-1) — ISM: molecules — molecular processes

1. INTRODUCTION

Among the molecules discovered in the interstellar medium, C_3H_2 and C_3H are of peculiar interest for astrochemistry since both are observed in two isomeric forms: cyclic and linear. The ring molecule cyclopropenylidene (hereafter c-C_3H_2) was discovered in 1985 (Thaddeus, Vrtilek, & Gottlieb 1985) and immediately gained attention because of its ubiquity in the Galaxy (e.g., Matthews & Irvine 1985). One of its linear counterparts, the propadienylidene (l-C_3H_2), was discovered in TMC-1 by Cernicharo et al. (1991). The two isomeric shapes of C_3H, cyclopropynylidyne (c-C_3H) and propynylidyne (l-C_3H), were also detected in TMC-1 (Yamamoto et al. 1987; Thaddeus et al. 1985).

This variety of isomers for the same species raises the question of their formation. In particular, are rings and chains formed from the same progenitors and involved in the same reactions networks? Furthermore, these isomers can be used to probe interstellar chemistry models that include heavy interstellar molecules such as cumulene carbenes (Bettens & Herbst 1996, 1997; see also Millar, Leung, & Herbst 1987). Previous observations by Cernicharo et al. (1999) have shown that the cyclic over linear abundance ratio of C_3H_2 (hereafter R_2) in the diffuse medium along the line of sight toward the continuum sources W51E1/E2, W51D, and W49 is 1 order of magnitude smaller than its value in TMC-1. In a recent study, Turner, Herbst, & Terzieva (2000) have compared measurements in three translucent clouds and two dense clouds (TMC-1 and L183) of the C_3H cyclic over linear abundance ratio (R_1) and R_2 ratio—and column densities of six other hydrocarbons—to a modified version of the New Standard Model of chemistry (Lee, Bettens, & Herbst 1996). They found small variation of R_1 from source to source and a systematic higher R_2 ratio, with the largest values found in the two dark clouds. Also, it has been suggested that cyclic and linear isomers of a same compound could have different behavior in neutral-neutral and ion-neutral reactions (see, e.g., Adams & Smith 1987; Maluendes, McLean, & Herbst 1993; Kaiser et al. 1997, 1999). The cyclic over linear abundance ratio of molecules such as C_3H_2 and C_3H could then be used as a tool to investigate physical conditions in several media, from cold dark cloud to warmer and lower density media.

To investigate these questions, we mapped in detail the region around the cyanopolyyne peak (hereafter CP) in TMC-1 in both l-C_3H_2 and c-C_3H_2 and observed at selected positions the two isomeric forms of C_3H. C_6H and HC_3N have also been observed for the purposes of comparison.

2. OBSERVATIONS

The C_3H_2 and C_6H observations were made in 1990 and 1992 with the 100 m telescope of the Max-Planck-Institut für Radioastronomie at Effelsberg (Germany). We observed the 1_{10}–1_{01} transitions of c-C_3H_2 at 18343.145 MHz and, simultaneously, those of C_6H $^2\Pi_{3/2}$ $J = 15/2$–$13/2$ near 20794 MHz and l-C_3H_2 1_{01}–0_{00} at 20792.590 MHz. The antenna beam sizes at 18.3 and 20.7 GHz are of 54″ and 48″, respectively. We used the 1024 channel autocorrelator to achieve a resolution of 0.05 km s^{-1} at 18.3 GHz and 0.09 km s^{-1} at 20.7 GHz, and the data were taken by position switching the telescope.

The HC_3N and C_3H observations were done in 1995 and 1999 with the IRAM 30 m telescope at Pico Veleta (Spain). We observed the l-C_3H $^2\Pi_{3/2}$ $J = 9/2$–$7/2$ transition near 98 GHz and, at the same time, the transition of c-C_3H 2_{12}–1_{11} near 91.5 GHz. The observations were made in frequency-switching mode. The autocorrelator was used as a spectral instrument with a velocity resolution of 0.12 km s^{-1}. The half-power beamwidth (HPBW) and main-beam efficiency are 26″ and 0.75 for l-C_3H and 27″ and 0.78 for c-C_3H. System temperatures were in the range of 90 to 130

[1] Depto Física Molecular, Instituto de Estructura de la Materia, Consejo Superior de Investigaciones Científicas, Serrano 121, E-28006 Madrid, Spain.

[2] Laboratoire de Radioastronomie Millimétrique, Observatoire de Paris and Ecole Normale Supérieure, 24 rue Lhomond, F-75231 Paris, CEDEX 05, France; David.Fosse@lra.ens.fr.

[3] Institut d'Astrophysique Spatiale, Université de Paris-Sud, Bâtiment 121, F-91405 Orsay, France.

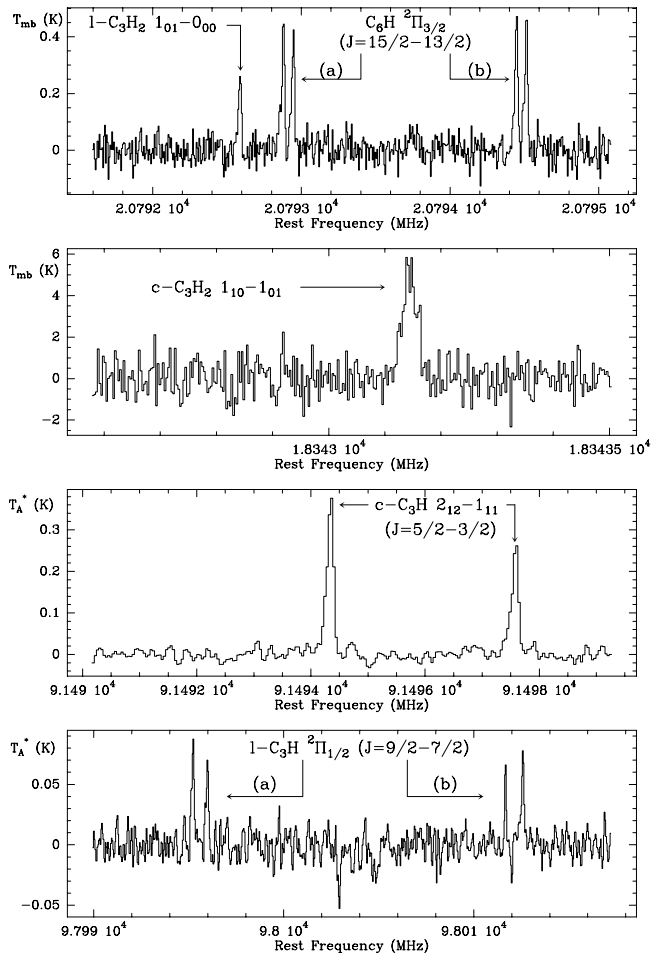

FIG. 1.—Spectra of C_6H, cyclic and linear C_3H_2, and cyclic and linear C_3H toward the CP of TMC-1 (v_{LSR} = 5.8 km s^{-1}). Note that the C_6H $^2\Pi_{3/2}$ J = 15/2–13/2 quadruplet and the l-C_3H_2 1_{01}–0_{00} transition are observed in the same bandwidth. The J = 3/2–1/2, F = 2–1, and F = 1–0 transitions of c-C_3H 2_{12}–1_{11} are not shown here.

K. For HC_3N, observed at 90979.023 MHz (J = 10–9), the HPBW is 26″. Pointing and calibration were monitored by regularly observing planets and quasars for both telescopes. Sample spectra are shown in Figure 1, and line parameters for selected positions are given in Table 1.

3. RESULTS

3.1. C_3H_2 *Isomers and* C_6H

The mapping results of this study are shown in Figure 2. The distributions toward the CP in TMC-1 of c-C_3H_2 and l-C_3H_2 are compared to that of C_6H in Figure 2*a* and 2*b*, respectively. Figure 2*c* shows the distributions of C_6H and HC_3N. The spatial distributions of l-C_3H_2 and c-C_3H_2 (Fig. 2*d*) are clearly different, whereas the emissions of c-C_3H_2, C_6H, and HC_3N have comparable distributions. The emission of l-C_3H_2 is shifted toward the west by approximately 40″ with respect to c-C_3H_2 or C_6H—note that, since C_6H and l-C_3H_2 were observed in the same bandwidth, this shift cannot be caused by pointing errors during the observations.

To derive relative abundances, we first computed relations between the column density and the observed line intensity valid for uniform physical conditions, i.e., $n(H_2)$ = 3×10^4 cm^{-3} and T_K = 10 K in TMC-1 (Cernicharo & Guélin 1987). From a statistical equilibrium calculation using collisional excitation rates for c-C_3H_2 from Avery & Green (1989), and assuming an ortho/para ratio of 3, we find: $N(c\text{-}C_3H_2)$ [cm^{-2}] = $2.2 \times 10^{13} \int T_{mb}\,dv$ [K km s^{-1}]. This linear relationship indicates that the 1_{10}–1_{01} transition of c-C_3H_2 is optically thin in TMC-1; it is in good agreement with the work of Cox, Walmsley, & Güsten (1989). Madden, Irvine, & Matthews (1986), from observations of the isotopic c-$C_2^{13}CH_2$ in TMC-1, derive an optical depth ranging from 5.6 to 6.8 for the 2_{12}–1_{01} transition of c-C_3H_2 at 85 GHz. This result is in agreement with ours since the 2_{12}–1_{01} line has a larger opacity than the 1_{10}–1_{01} transition for dark cloud physical conditions. Indeed, with our code, we are able to reproduce the results of Madden et al. at 85 GHz, the 1_{10}–1_{01} transition still being thin or marginally saturated ($\tau \leq 1.5$). For l-C_3H_2 and C_6H, there are no collisional cross sections available. We have estimated cross sections from those of H_2CO (calculated by Green et al. 1978) and of HC_3N (Green & Chapman 1978)—see Cernicharo et al. (1999). This gives $N(l\text{-}C_3H_2)$ [cm^{-2}] = 2.2 $\times 10^{13} \int T_{mb}\,dv$ [K km s^{-1}] and $N(C_6H)$ [cm^{-2}] = 5.2 $\times 10^{13} \int T_{mb}\,dv$ [K km s^{-1}]. Note that for C_6H, $\int T_{mb}\,dv$ is the total integrated intensity summed over the four components of the hyperfine structure. These relationships are in good agreement with previous works (Cernicharo et al. 1991; Bell et al. 1999).

TABLE 1

LINE PARAMETERS FOR C_6H, l-C_3H_2, AND c-C_3H_2 AT SELECTED POSITIONS IN TMC-1

	C_6H			l-C_3H_2				c-C_3H_2		
POSITION (arcsec)	T_{mb} (K)	v_{LSR} (km s^{-1})	Δv (km s^{-1})	T_{mb} (K)	v_{LSR} (km s^{-1})	Δv (km s^{-1})	POSITION (arcsec)	T_{mb} (K)	v_{LSR} (km s^{-1})	Δv (km s^{-1})
0, 0	0.41 ± 0.02	5.72 ± 0.01	0.27 ± 0.02	0.27 ± 0.03	5.83 ± 0.02	0.33 ± 0.03	0, 0	3.69 ± 0.59	5.54 ± 0.01	0.12 ± 0.02
	0.13 ± 0.02	6.02 ± 0.05	0.29 ± 0.07	...	...	...		4.44 ± 0.59	5.72 ± 0.01	0.14 ± 0.02
	...	...	...	...	...	...		5.46 ± 0.59	5.89 ± 0.02	0.20 ± 0.02
	...	...	...	...	...	...		2.46 ± 0.59	6.12 ± 0.02	0.14 ± 0.03
−40, 0	0.31 ± 0.03	5.74 ± 0.01	0.25 ± 0.00	0.31 ± 0.07	5.78 ± 0.03	0.44 ± 0.08	−50, 0	2.20 ± 0.76	5.48 ± 0.05	0.20 ± 0.00
	0.11 ± 0.11	5.99 ± 0.02	0.09 ± 0.20	...	...	...		3.99 ± 0.76	5.70 ± 0.03	0.20 ± 0.00
0, 40	0.29 ± 0.04	5.82 ± 0.03	0.21 ± 0.06	0.28 ± 0.06	5.85 ± 0.02	0.18 ± 0.04	0, 50	3.96 ± 0.71	5.68 ± 0.02	0.17 ± 0.04
	0.25 ± 0.04	6.07 ± 0.04	0.21 ± 0.09	0.26 ± 0.06	6.15 ± 0.02	0.14 ± 0.04		4.58 ± 0.71	5.96 ± 0.02	0.28 ± 0.05
40, −40	0.48 ± 0.03	5.78 ± 0.01	0.25 ± 0.00	0.28 ± 0.07	5.80 ± 0.03	0.21 ± 0.06	50, −50	2.83 ± 0.78	5.61 ± 0.03	0.19 ± 0.05
	0.22 ± 0.03	6.03 ± 0.03	0.27 ± 0.05	0.23 ± 0.07	6.08 ± 0.03	0.13 ± 0.06		4.88 ± 0.78	5.88 ± 0.03	0.34 ± 0.06

NOTE.—Positions are offsets relative to the CP: α(1950) = 04^{h}38^{m}38^s.6, δ(1950) = 25°35′45″.0. TMC-1 exhibits two main components at $v_{LSR} \simeq$ 5.3 and 6.1 km s^{-1} (Sume, Downes, & Wilson 1975). When possible, we have fitted several components along a line of sight.

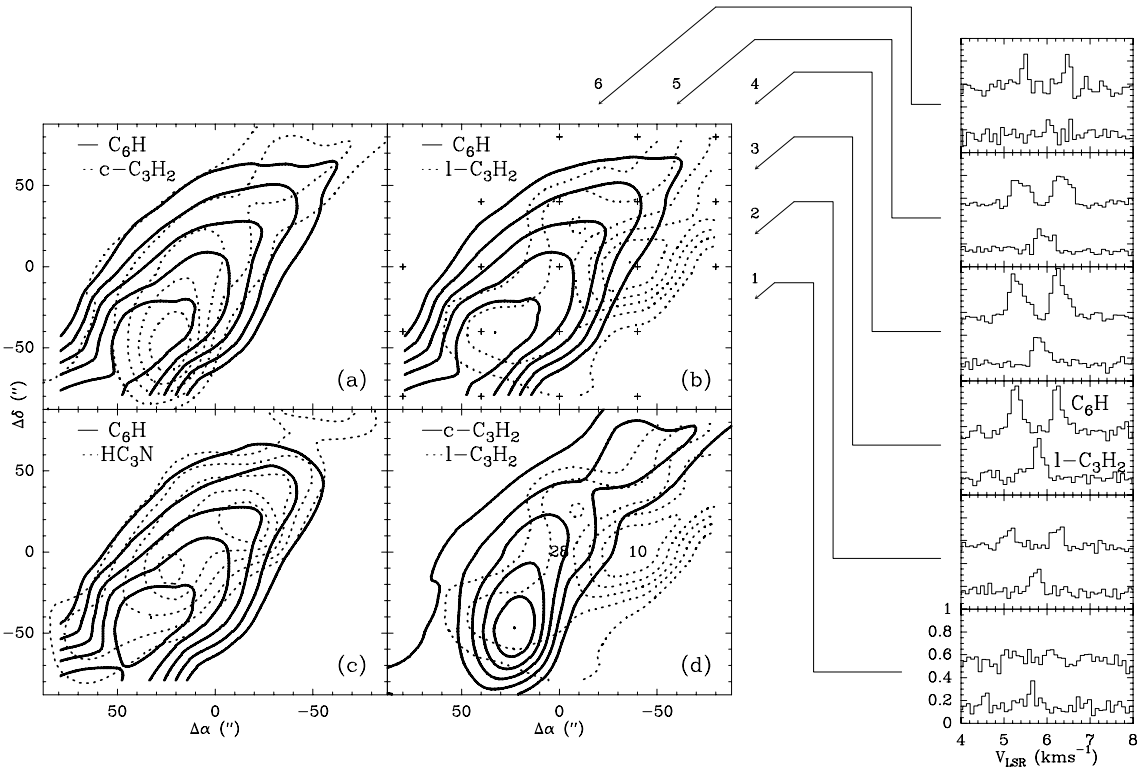

FIG. 2.—Contour levels of integrated intensity in TMC-1 for (*a*) C_6H $^2\Pi_{3/2}$ $J = 15/2$–$13/2$ and *c*-C_3H_2 1_{10}–1_{01}; (*b*) C_6H $^2\Pi_{3/2}$ $J = 15/2$–$13/2$ and *l*-C_3H_2 1_{01}–0_{00} (the crosses indicate the measured positions); (*c*) C_6H $^2\Pi_{3/2}$ $J = 15/2$–$13/2$ and HC_3N 10–9; (*d*) *c*-C_3H_2 1_{10}–1_{01} and *l*-C_3H_2 1_{01}–0_{00} [numbers indicate the values of R_2, i.e., the ratio $N(c\text{-}C_3H_2)/N(l\text{-}C_3H_2)$]. All contours go from 50% to 100% of the peak value by steps of 10%. Peak values are 0.16 K km s^{-1}, 2.6 K km s^{-1}, 0.15 K km s^{-1}, and 1.75 K km s^{-1} for C_6H, *c*-C_3H_2, *l*-C_3H_2, and HC_3N, respectively. Coordinates of the (0, 0) position are: $\alpha = 04^h38^m38^s.6$, $\delta = 25°35'45''.0$ (1950.0) corresponding to the CP. Boxes to the right compare the C_6H and *l*-C_3H_2 spectra averaged along the six directions indicated by the arrows. Note the significant emission of *l*-C_3H_2 toward the west side of the TMC-1 filament where the emission of C_6H decreases rapidly.

Comparing two positions separated by 40″ (which corresponds to 0.02 pc for the adopted distance of 100 pc to TMC-1; Cernicharo & Guélin 1987), we derive the following column density: at the CP (0, 0), $N(C_6H) = 8.3 \times 10^{12}$ cm^{-2}, $N(c\text{-}C_3H_2) = 5.8 \times 10^{13}$ cm^{-2}, $N(l\text{-}C_3H_2) = 2.1 \times 10^{12}$ cm^{-2} ($R_2 = 28 \pm 6$); and at the edge of the TMC-1 filament (−40, 0), $N(C_6H) = 4.7 \times 10^{12}$ cm^{-2}, $N(c\text{-}C_3H_2) = 2.8 \times 10^{13}$ cm^{-2}, $N(l\text{-}C_3H_2) = 3.2 \times 10^{12}$ cm^{-2} ($R_2 = 10 \pm 3$). Between these two positions, the cyclic over linear abundance ratio changes by a factor of ~ 3. This variation cannot be an artifact caused by calibration errors. Indeed, while the calculated C_6H over *l*-C_3H_2 column-density ratio varies from 1.5 to 4, the *c*-C_3H_2 over C_6H column-density ratio remains constant ($\simeq 6.5$). Since the former ratio is unaffected by calibration and pointing errors (lines are observed in the same bandwidth), the observed variation of R_2 must be real. This result suggests that chemical gradients are present in TMC-1 on scales smaller than 0.02 pc.

To investigate further the spatial variations of molecular abundances across the TMC-1 filament, we averaged the spectra along the six different rows shown in Figure 2. Results are summarized in Figure 3: R_2 ranges from 12 to 37 and clearly increases from the west to the east of TMC-1. Note that a constant density of $n(H_2) = 3 \times 10^4$ cm^{-3} has been adopted. If we use instead H_2 densities derived by Pratap et al. (1997) from an analysis of the HC_3N transitions while keeping the same kinetic temperature (10 K), the values of R_2 are then lowered by 20% to 40%, but the west to east variation of R_2 remains. The rise of the cyclic over linear abundance ratio of the C_3H_2 isomers at a spatial scale of 2′ (0.06 pc) is therefore a firm result.

3.2. C_3H *Isomers*

As C_3H is thought to be formed by the same reaction as C_3H_2, i.e., by the dissociative recombination of $C_3H_3^+$ (Adams & Smith 1987), it is interesting to compare $N(c\text{-}C_3H)/N(l\text{-}C_3H)$ (hereafter R_1) with R_2. What is the value of R_1 and does it vary across the filament similarly to R_2? To answer these questions, we observed *c*-C_3H and *l*-C_3H at 13 positions along two strips close to the CP. One strip crosses the filament from offset positions (60″, 60″) to (−60″, −60″), the other from (10″, −70″) to (−70″, 10″). We also observed the *c*-C_3H_2 and the *l*-C_3H_2 peaks. Where possible, we analyzed the data with the HyperFine Structure method of CLASS (a software developed by the Grenoble Image and Line Data Analysis Software working group). This method provides the total optical depth, the average line width, and the brightness temperature of a line with hyperfine structure. A reliable estimate of the excitation temperature could be obtained for several points. We found 3 K $\leq T_{ex} \leq$ 3.8 K for *c*-C_3H (in excellent agreement with Mangum & Wootten 1990) and 4.9 K $\leq T_{ex} \leq$ 6.7 K for *l*-C_3H. In the following, we adopt $T_{ex} = 3.5$ K for *c*-C_3H and $T_{ex} = 5.5$ K for the linear isomer.

Calculations of the column densities were done using the classical formula with $\mu = 2.4$ D (Yamamoto et al. 1987) for *c*-C_3H and $\mu = 3.1$ D (Green 1980) for *l*-C_3H. For each

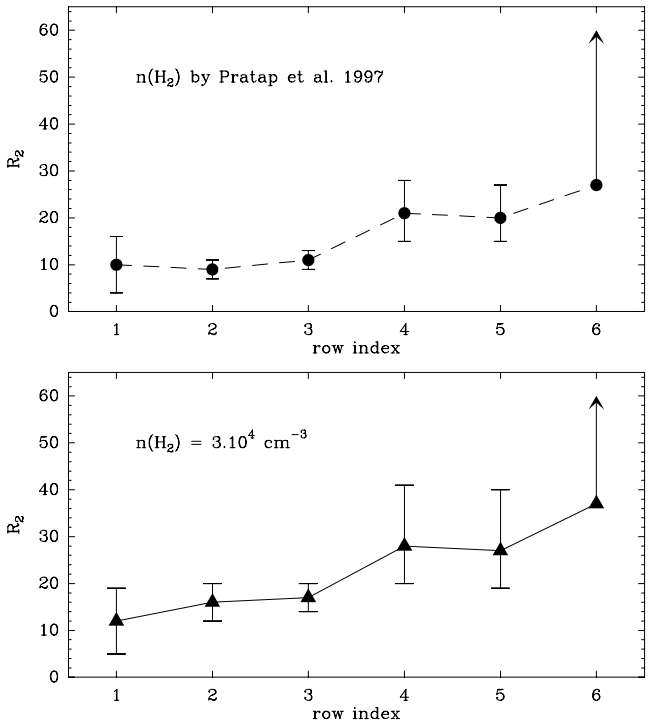

FIG. 3.—Variations of R_2 [i.e., the ratio $N(c\text{-}C_3H_2)/N(l\text{-}C_3H_2)$] across the TMC-1 filament using (*lower panel*) a constant density of 3×10^4 cm^{-3}; densities in the upper panel have been derived by Pratap et al. (1997). To increase the signal-to-noise ratio, the spectra have been averaged along six rows (separated by 28″) parallel to the TMC-1 filament. Lower limits in row number 6 are derived from 3 σ upper limits on the l-C_3H_2 emission. The CP is located within row number 4.

observed point, we computed the average of the total column densities by using each hyperfine transition weighted by the inverse of the square of the error. The resulting column densities and the values for R_1 are given in Table 2. Comparing with the values of R_2 in Figure 3, we see that (1) with a value of 12 at the CP, R_1 is smaller than R_2; and (2) as R_2 does, R_1 shows variations across the filament (by a factor of 2.5), mainly because of variations of $N(c\text{-}C_3H)$.

TABLE 2

DERIVED COLUMN DENSITIES FOR c-C_3H AND l-C_3H IN TMC-1

Position (arcsec)	$N(c\text{-}C_3H)$ (10^{12} cm^{-2})	$N(l\text{-}C_3H)$ (10^{11} cm^{-2})	Nc/Nl ($= R_1$)
−40, −40.....	3.7 ± 0.2	≤4	≥9
−20, −20.....	7.7 ± 0.3	8.0 ± 0.2	10 ± 0.5
0, 0.....	10.3 ± 0.3	8.4 ± 0.1	12 ± 0.5
20, 20.....	10.0 ± 0.3	7.6 ± 0.4	13 ± 1.2
40, 40.....	5.8 ± 0.3	6.7 ± 0.5	9 ± 1.1
60, 60.....	3.6 ± 0.2	6.1 ± 0.7	6 ± 1.0
10, −70.....	5.2 ± 0.2	7.0 ± 0.4	7 ± 0.6
−10, −50.....	5.3 ± 0.2	7.8 ± 0.2	7 ± 0.4
−30, −30.....	5.1 ± 0.2	8.0 ± 0.1	6 ± 0.4
−50, −10.....	4.7 ± 0.2	7.1 ± 0.5	7 ± 0.8
−70, 10.....	3.7 ± 0.2	7.3 ± 0.3	5 ± 0.5
30, −60[a].....	7.8 ± 0.3	8.0 ± 0.2	10 ± 0.6
−30, 0[b].....	10.0 ± 0.4	8.2 ± 0.2	12 ± 0.7

NOTE.—Positions are offsets relative to the CP: $\alpha(1950) = 04^h38^m38^s.6$, $\delta(1950) = 25°35'45''.0$.

[a] c-C_3H_2 peak.

[b] l-C_3H_2 peak.

4. DISCUSSION

The observations described above underscore the differences in the distribution and relative abundances of the cyclic and linear forms of C_3H_2 and C_3H in the molecular filament TMC-1. In the following, we study the origin of this behavior and suggest that it is driven by competitive processes between ion-neutral and neutral-neutral reactions.

4.1. *Steady State Calculation*

We assume here, as it has been proposed (see, e.g., Adams & Smith 1987; Maluendes et al. 1993), that cyclic C_3H_2 and C_3H are both formed in the dissociative recombination of c-$C_3H_3^+$, while linear C_3H_2 and C_3H result from $H_2C_3H^+$. We also assume that the $C_3H^+ + H_2$ association reaction is the dominant formation mechanism of $C_3H_3^+$, which is produced in equal amounts in cyclic and linear forms.

At steady state, the chemical kinetic equation for the abundance of c-C_3H_2—that is, $x(c\text{-}C_3H_2)$—is

$$dx(c\text{-}C_3H_2)/dt = {}^2b_c\, k_c^r\, x(c\text{-}C_3H_3^+)x_e - {}^2K_c^d\, x(c\text{-}C_3H_2) = 0\ ,$$

where b is the branching ratio, k^r is the recombination rate [cm^3 s^{-1}], K^d is the mean destruction rate [s^{-1}] ($K^d = \sum_i k_i^d x_i$, where x_i is the second reactant). We use indices (l, c) and exponents (2, 1) to distinguish between C_3H_2 and C_3H in linear and cyclic forms (for example, ${}^2b_c$ means "branching ratio for cyclic C_3H_2"). Similar equations can be written for l-C_3H_2, c-C_3H, and l-C_3H. Using the observed column densities for each species at the border of the filament (i.e., row number 2), where the electron density should be the highest in our data set, and writing $k_c^r = k_l^r$ and $X \equiv x(c\text{-}C_3H_3^+)/x(l\text{-}C_3H_3^+)$, calculations lead to

$$x(c\text{-}C_3H_2)/x(c\text{-}C_3H) = ({}^2b_c/{}^1b_c)({}^1K_c^d/{}^2K_c^d) \simeq 5\ ;$$

$$x(l\text{-}C_3H_2)/x(l\text{-}C_3H) = ({}^2b_l/{}^1b_l)({}^1K_l^d/{}^2K_l^d) \simeq 2\ ;$$

$$R_2 = ({}^2b_c/{}^2b_l)({}^2K_l^d/{}^2K_c^d)X \simeq 16\ ;$$

$$R_1 = ({}^1b_c/{}^1b_l)({}^1K_l^d/{}^1K_c^d)X \simeq 6\ .$$

A simple and coherent set of solutions for this system is ${}^2b_l \simeq {}^1b_l \simeq {}^1b_c \simeq {}^2b_c$; ${}^1K_l^d \simeq 2\ {}^2K_l^d$; ${}^1K_c^d \simeq 5\ {}^2K_c^d$; ${}^1K_c^d \simeq (\frac{1}{6})\ {}^1K_l^d\, X$; ${}^2K_c^d \simeq (\frac{1}{16})\ {}^2K_l^d\, X$.

Under the hypothesis of steady state and from the observed abundance ratio at the border of the TMC-1 filament, we find that c-C_3H_2 is destroyed approximately 5 times slower than c-C_3H and that the l-C_3H mean destruction rate is twice the l-C_3H_2 one.

To our knowledge, no additional formation process of c-C_3H_2 in dark clouds can be invoked to explain an increase of its abundance with respect to l-C_3H_2. Variations of R_2 (and R_1) in TMC-1 could result from variations of the destruction rates of c-C_3H_2 and l-C_3H_2. Such an explanation has been proposed by Maluendes et al. (1993): while c-C_3H_2 is inert with respect to most neutral-neutral reactions, l-C_3H_2, as l-C_3H and c-C_3H, are easily destroyed by these reactions. Hence, because neutral-neutral reactions proceed quickly when a radical reacts with abundant atoms, it is possible in a dark cloud such as TMC-1 that R_2 is 1 order of magnitude larger than in a more diffuse medium where the proportion of reactive ions (increasing with respect to reactive atoms) is sufficient to destroy c-C_3H_2 and l-C_3H_2 at the same rate. The same explanation holds for the progenitor ions c-$C_3H_3^+$ and l-$C_3H_3^+$ (see

Cernicharo et al. 1999): while l-$C_3H_3^+$—assumed to be the progenitor of l-C_3H_2—can be efficiently removed through ion-neutral reactions lowering the amount available to produce l-C_3H_2, c-$C_3H_3^+$ is affected mainly by dissociative recombination to produce c-C_3H_2. R_2 thus depends on the ion-neutral reactions of l-$C_3H_3^+$ that do not affect the cyclic ion: in dark clouds, where the abundance of reactive molecules can be a hundred times larger than that of electrons, l-$C_3H_3^+$ is removed faster by ion-neutral reactions than by the dissociative recombination lowering the production rate of l-C_3H_2 and increasing R_2. In a more diffuse medium, where the ion-neutral reactions are much less efficient, l-$C_3H_3^+$ and c-$C_3H_3^+$ are removed by the same process and R_2 is then closer to ${}^2K_l^d/{}^2K_c^d$ (the value of which also decreases with decreasing density, as suggested above). This explanation is strengthened by the lower R_2 values found in the diffuse medium from absorption measurements by Cernicharo et al. (1999)—3 to 5 versus 10 to 40 in TMC-1—and by the observed R_1 variations across the filament. We test this hypothesis in the next section.

4.2. *Chemical Modeling*

To study the impact of physical conditions on the R_2 ratio, we have run 25 models of gas phase chemistry with different densities and visual extinctions using a time-dependent chemistry code solving the system of stiff ordinary differential equations with the Gear method. Although we have used a time-dependent chemistry code—samples of the evolution chemistry are shown in Figure 4—we discuss here the results at steady state. Indeed, we would like to study the basic processes of the isomeric differentiation and identify the dominant reactions leading to the observed large variations of R_2 in diffuse and dense clouds. We aim first at a qualitative description of the mechanism. A quantitative description would require a more accurate knowledge of the reaction rates (including branching ratios) important for c-C_3H_2 and l-C_3H_2. Figure 4 shows that c-C_3H_2/l-C_3H_2 and c-$C_3H_3^+$/l-$C_3H_3^+$ abundance ratios reach values close to the steady state value, just after they rise to their maximum abundance. As a first step, it is thus reasonable to consider only the processes leading to variation in isomeric abundances at steady state. We have used, as a chemical network, the UMIST95 database (Millar, Farquhar, & Willacy 1997) in a pure gas-phase scheme. As recommended by the authors, the species C_2H_5, C_2H_6 and their ions have been excluded from the network. We have also excluded the species including the following atoms: P, Si, Cl, Na, Mg. On the other hand, we have included the grain surface formation of H_2 with a rate coefficient $1.5 \times 10^{-17}\ n^2(\mathrm{H})\ \mathrm{cm}^{-3}\ \mathrm{s}^{-1}$. Moreover, we have updated the dissociative recombination rate of c-$C_3H_3^+$ at 300 K to $7.0 \pm 2.0 \times 10^{-7}\ \mathrm{cm}^3\ \mathrm{s}^{-1}$ (Abouelaziz et al. 1993) and assumed the same value for l-$C_3H_3^+$. Parameters of the models and initial elemental abundances are given in Tables 3 and 4, respectively.

In Figure 4, we see that R_2 and also X increase with increasing visual extinction. This general trend of our models agrees with observations since R_2 is lower in the

TABLE 3

PARAMETERS OF THE CHEMICAL MODELS

Parameter	Value
$n(H_2)$ (10^3 cm^{-3}).....	1, 3, 10, 30, 100
T (K).....	10
A_V (mag).....	1 , 2 , 3 , 5 , 10
ζ (s^{-1})[a].....	1.3×10^{-17}
u_i (ergs cm^{-3})[b]	2×10^{-15}

[a] ζ is the cosmic-ray ionization rate.
[b] u_i is the density of ionizing radiation at $A_V = 0$.

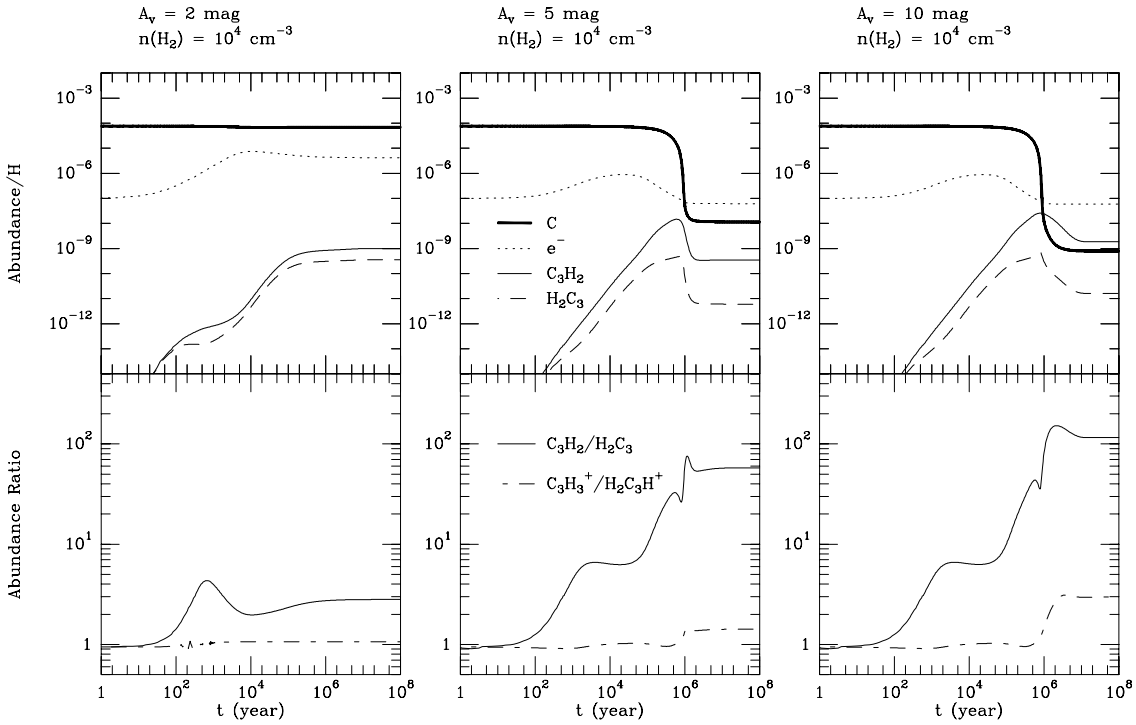

FIG. 4.—Chemical evolution for three different visual extinctions at $n(H_2) = 10^4$ cm^{-3} and $T = 10$ K. Upper boxes show abundances relative to H for C, l-C_3H_2, c-C_3H_2, and e^-. Lower boxes show the resulting cyclic over linear abundance ratio for C_3H_2 and $C_3H_3^+$ isomers.

TABLE 4

INITIAL ELEMENTAL ABUNDANCES WITH RESPECT TO HYDROGEN

Element	Value
He.....	1.4×10^{-1}
C	7.3×10^{-5}
N	2.14×10^{-5}
O	1.76×10^{-4}
S.....	2.0×10^{-8}
Fe	3.0×10^{-9}

diffuse medium than in the TMC-1 dark cloud. The models also show that the increase is faster in higher density media. We have plotted in Figure 5 the electronic density with respect to R_2 for each model. The distribution of the points exhibits clearly a correlation between the ionization fraction and the cyclic over linear ratio that can be separated in two regimes: "low" ($1 \leq A_V \leq 2$) and "high" ($5 \leq A_V \leq 10$), $A_V = 3$ mag being an intermediate case. In the low extinction regime, R_2 strongly depends on the electronic abundance. This is an interesting result because it opens the possibility to use R_2 as a tool to probe the electronic abundance in low extinction regions where $H^{13}CO^+$ and DCO^+ cannot be detected. Why is the cyclic over linear ratio sensitive to the ionization fractionation? In the UMIST95 chemistry, C^+ can destroy both l-C_3H_2 and c-C_3H_2, whereas C reacts only with the linear isomer. R_2 is then sensitive to the electronic abundance *via* the C^+/C ratio as shown in Figure 6. Note that the range 3–5 that Cernicharo et al. (1999) have observed in the diffuse medium corresponds, as expected, to high electronic abundances and to moderate visual extinctions. In the high extinction regime, R_2 is independent of the C^+/C ratio while it is sensitive to the $(H_3^+ + C^+)/O$ ratio (Fig. 7). Indeed, in the UMIST95 database, the atomic oxygen reacts only with l-C_3H_2 ($O + l\text{-}C_3H_2 \rightarrow C_2H_2 + CO$).

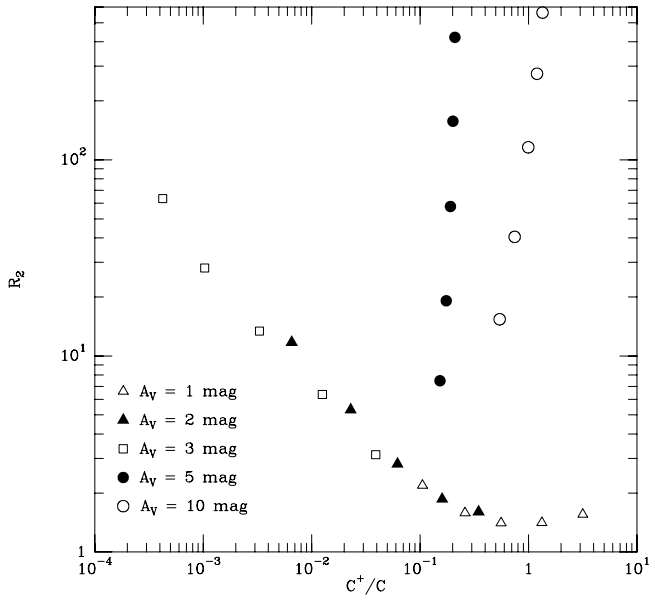

FIG. 6.—Predicted dependence of R_2 with the C^+/C ratio at steady state. A clear relationship is established at low visual extinction between R_2 and the ionization fraction of atomic carbon. Note that at high visual extinctions R_2 depends only weakly on C^+/C.

This reaction is negligible with respect to other destruction reactions (in particular, the reactions with C^+, which affects both isomers) until all the carbon is locked into CO. It is thus inefficient in low visual extinction media where the abundances of C and C^+ remain high. On the other hand, it becomes the principal destruction channel of l-C_3H_2 at high visual extinctions: for $A_V = 2$ mag and a density of 10^3 cm^{-3}, the $O + l$-C_3H_2 reaction is roughly 15% of the l-C_3H_2 destruction rate while it represents more than 80% of it at $A_V = 10$ mag. The variations of the cyclic over linear abundance ratio of C_3H_2 can thus be under-

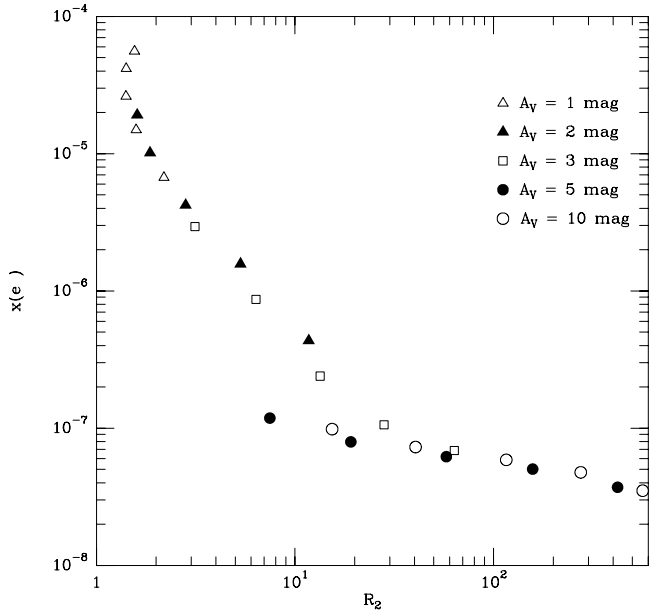

FIG. 5.—Predicted electronic abundance vs. R_2 at steady state. Two regimes can be distinguished accordingly as the visual extinction is low or high.

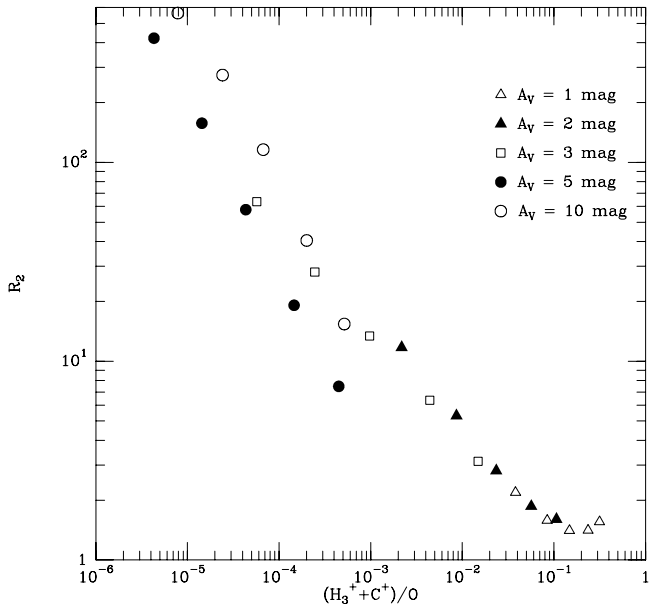

FIG. 7.—Model prediction for the relation of R_2 vs. the $(H_3^+ + C^+)/O$ ratio at steady state. Note the good correlation between R_2 and $(H_3^+ + C^+)/O$ at high visual extinctions.

stood as a consequence of the competition between neutral-neutral and ion-neutral reactions in the interstellar medium.

The determination of electronic abundances from measurements of R_2 using Figure 5 may not be straightforward. Indeed, taking into account the large uncertainties in the reaction rates and branching ratios, it is difficult to infer quantitative results from this study on the C_3H_2 isomers. We can say, however, that low R_2 values are specific of high electronic abundance while high R_2 values indicate low electronic abundance. In a more general way, isomeric ratios can be used to probe physical conditions in different media from the diffuse gas to dark clouds. In the future, cyclic and linear species other than the isomers of C_3H_2 shall be included in chemical models. C_3H is a good candidate. Indeed, Kaiser et al. (1997, 1999) have shown that the neutral-neutral reaction $C + C_2H_2 \rightarrow C_3H + H$ produces linear and cyclic C_3H, with an increase of the linear over cyclic abundance ratio with rising collision energies. It would be interesting to make measurements of R_1 in absorption in the diffuse medium in order to compare this neutral-neutral formation path with the $C_3H_3^+$ dissociative recombination.

This study has been partly begun. Indeed, in a recent paper, Turner, Herbst, & Terzieva (2000) investigate the R_1 and R_2 ratios in three translucent clouds and in the dark clouds TMC-1 and L183. They compare observations to the predictions of a modified version of the New Standard Model of chemistry (Lee et al. 1996), which includes cyclic and linear species for all precursors to C_3H and C_3H_2. One of their conclusions is that the clear observed anti-correlation of R_2 with extinction suggests that the ratios are strongly affected by formation or destruction rates and not just by branching ratios among the relevant chemical reactions.

5. CONCLUSION

In this paper, we have presented new results about the cyclic over linear abundance ratios of C_3H_2 and C_3H toward the CP of TMC-1. These ratios exhibit variations, which are probably caused by variations in the electronic abundance across the filament. Indeed, the chemical modeling of the reactions that affect c-C_3H_2 and l-C_3H_2 shows that their ratio is sensitive mainly to the behavior of the C^+/C (at low visual extinction) and $(H_3^+ + C^+)/O$ (at high visual extinction) abundance ratios, which are both related to the electronic abundance. As C_3H_2 is observed in its cyclic and linear form in different physical conditions, it could be used as a tool to probe the electronic abundance in the ISM. However, to infer accurate values of the fractional ionization from cyclic and linear isomers abundances, the branching ratios and kinetic rates used in chemical networks must be more accurately known. In addition to laboratory studies, a systematic measurement of R_1 and R_2 in different astrophysical media should be useful for this work.

We thank C. M. Walmsley for useful comments and suggestions. D. F. and J. C. thank the Spanish DGCYT for funding under grants PB96-0883 and PNIE98-1351E. D. F. also acknowledges the Spanish Ministry of Foreign Affairs for support under grant 195.

REFERENCES

Abouelaziz, H., Gomet, J. C., Pasquerault, D., Rowe, B. R., & Mitchell, J. B. A. 1993, J. Chem. Phys., 98, 1
Adams, N. G., & Smith, D. 1987, ApJ, 317, L25
Avery, L. W., & Green, S. 1989, ApJ, 337, 306
Bell, M. B., Feldman, P. A., Watson, J. K. G., McCarthy, M. C., Travers, M. J., Gottlieb, C. A., & Thaddeus, P. 1999, ApJ, 518, 740
Bettens, R. P. A., & Herbst, E. 1996, ApJ, 468, 686
———. 1997, ApJ, 478, 585
Cernicharo, J., Cox, P., Fossé D., & Güsten, R. 1999, A&A, 351, 341
Cernicharo, J., Gottlieb, C. A., Guélin, M., Killian, T. C., Paubert, G., Thaddeus, P., & Vrtilek, J. M. 1991, ApJ, 368, L39
Cernicharo, J., & Guélin, M. 1987, A&A, 176, 299
Cox, P., Walmsley, C. M., & Güsten, R. 1989, A&A, 209, 382
Green, S. 1980, ApJ, 240, 962
Green, S., & Chapman, S. 1978, ApJS, 37, 169
Green, S., Garrison, B. J., Lester, W. A., Jr., & Miller, W. H. 1978, ApJS, 37, 321
Kaiser, R. I., Ochsenfeld, C., Head-Gordon, M., & Lee, Y. T. 1999, ApJ, 510, 784
Kaiser, R. I., Stranges, D., Lee, Y. T., & Suits, A. G. 1997, ApJ, 477, 982
Lee, H.-H., Bettens, R. P. A., & Herbst, E. 1996, A&AS, 119, 111
Madden, S. C., Irvine, W. M., & Matthews, H. E. 1986, ApJ, 311, L27
Maluendes, S. A., McLean, A. D., & Herbst, E. 1993, ApJ, 417, 181
Mangum, J. G., & Wootten, A. 1990, A&A, 239, 319
Matthews, H. E., & Irvine, W. M. 1985, ApJ, 298, L61
Millar, T. J., Farquhar, P. R. A., & Willacy, K. 1997, A&AS, 121, 139
Millar, T. J., Leung, C. M., & Herbst, E. 1987, A&A, 183, 109
Pratap, P., Dickens, J. E., Snell, R. L., Miralles, M. P., Bergin, E. A., Irvine, W. M., & Schloerb, F. P. 1997, ApJ, 486, 862
Sume, A., Downes, D., & Wilson, T. L. 1975, A&A, 39, 435
Thaddeus, P., Gottlieb, C. A., Hjalmarson, A., Johansson, L. E. B., Irvine, W. M., Friberg, P., & Linke, R. A. 1985, ApJ, 294, L49
Thaddeus, P., Vrtilek, J. M., & Gottlieb, C. A. 1985, ApJ, 299, L63
Turner, B. E., Herbst, E., & Terzieva, R. 2000, ApJS, 126, 427
Yamamoto, S., Saito, S., Ohishi, M., Suzuki, H., Ishikawa, S.-I., Kaifu, N., & Murakami, A. 1987, ApJ, 322, L55